Hydrogen Bonding to P700: Site-Directed Mutagenesis of Threonine A739 of Photosystem I in *Chlamydomonas reinhardtii*[†,‡]

Heike Witt,*[,§] Eberhard Schlodder,[§] Christian Teutloff,[§] Jens Niklas,[§,||] Enrica Bordignon,[⊥] Donatella Carbonera,[⊥] Simon Kohler,[@] Andreas Labahn,[@] and Wolfgang Lubitz*[,§,||]

Max-Volmer-Laboratorium für Biophysikalische Chemie, Technische Universität Berlin, Strasse des 17. Juni 135, 10623 Berlin, Germany, Max-Planck-Institut für Strahlenchemie, Stiftstrasse 34-36, 45470 Mülheim/Ruhr, Germany, Dipartimento di Chimica Fisica, Università di Padova, Via Loredan 2, 35131 Padova, Italy, and Institut für Physikalische Chemie, Universität Freiburg, Albertstrasse 23a, 79104 Freiburg, Germany

Received March 15, 2002; Revised Manuscript Received May 24, 2002

ABSTRACT: The primary electron donor P700 of photosystem I is a dimer comprised of chlorophyll *a* (P_B) and chlorophyll *a*′ (P_A). P_A is involved in a hydrogen bond network with several surrounding amino acid residues and a nearby water molecule. To investigate the influence of hydrogen bond interactions on the properties of P700, the threonine at position A739, which donates a putative hydrogen bond to the 13^1-keto group of P_A, was replaced with valine, histidine, and tyrosine in *Chlamydomonas reinhardtii* using site-directed mutagenesis. Growth of the mutants was not impaired. (i) The ($P700^{+\bullet}$ − P700) FTIR difference spectra of the mutants lack a negative band at 1634 cm^{-1} observed in the wild-type spectrum and instead exhibit a new negative band between 1658 and 1672 cm^{-1} depending on the mutation. This band can therefore be assigned to the 13^1-keto group of P_A which is upshifted to higher frequencies upon removal of the hydrogen bond. (ii) The main bleaching band in the Q_y region of the ($P700^{+\bullet}$ − P700) and (^{3}P700 − P700) absorption difference spectra is blue shifted for the mutants by ∼6 nm compared to that of the wild type. A blue shift is also observed for the main bleaching in the Soret region. (iii) The ($P700^{+\bullet}$ − P700) CD difference spectrum of the wild type reveals two bands at 694 nm (positive CD) and 680 nm (negative CD) of approximately equal area. For each mutant, these two components are blue-shifted to the same extent. The results strongly suggest that a blue shift of the Q_y absorption band of P_A is responsible for a blue shift of the exciton bands. (iv) Redox titrations yielded a decrease in the midpoint potential for the oxidation of P700 by 32 mV for the exchange of Thr against Val. (v) ENDOR spectroscopy shows that the hfc of the methyl protons at position 12 of the spin-carrying Chl P_B is decreased due to the removal of the hydrogen bond to P_A. This indicates a redistribution of spin density in $P700^{+\bullet}$ compared to that in the wild type. This gives evidence for an electronic coupling between the two halves of the dimer in the wild type and mutants.

Photosystem I (PSI)[1] of plants, algae, and cyanobacteria is a membrane-bound pigment−protein complex that mediates light-induced electron transfer from plastocyanin or cytochrome c_6 on the lumenal side to ferredoxin on the stromal side (for a review, see refs *1* and *2*). In plants and algae, PSI is composed of at least 13 subunits and associated with a light-harvesting complex (LHC-1). The subunits PsaA and PsaB, each consisting of 11 transmembrane helices, form the heterodimeric core and coordinate most of the cofactors involved in the electron transfer process and the main part of the antenna system with ∼100 chlorophylls and 20 β-carotenes. Only the terminal electron acceptors F_A and F_B (two [4Fe-4S] iron−sulfur clusters) are bound by one of the extrinsic subunits on the stromal side, PsaC. After absorption of light by an antenna pigment, the excitation energy is transferred to the primary electron donor P700, an excitonically coupled dimer which, being in the lowest excited singlet state, donates an electron to the primary electron acceptor A_o, a chlorophyll *a* monomer. Charge stabilization is achieved by subsequent electron transfer to secondary acceptors, the phylloquinone A_1 and F_x, a [4Fe-4S] iron−sulfur cluster, and finally to F_A and F_B.

The X-ray crystallographic analysis of cyanobacterial PSI (*3*) has revealed that the primary electron donor P700 of photosystem I is a dimer comprised of one chlorophyll *a* and one chlorophyll *a*′ which is the 13^2 epimer of Chl *a*

[†] This work was supported by Sfb 498 (TPC5 and TPA1) and the TMR programme (FMRX-CT98-0214).

[‡] This paper is dedicated to Prof. H. T. Witt on the occasion of his 80th birthday.

* To whom correspondence should be addressed. H.W.: e-mail, heike@struktur.chem.tu-berlin.de. W.L.: e-mail, lubitz@mpi-muelheim.mpg.de.

[§] Technische Universität Berlin.

[||] Max-Planck-Institut für Strahlenchemie.

[⊥] Università di Padova.

[@] Universität Freiburg.

[1] Abbreviations: ADMR, absorption-detected magnetic resonance; BChl, bacteriochlorophyll; Chl, chlorophyll; CD, circular dichroism; DM, *n*-dodecyl β-maltoside; ENDOR, electron nuclear double resonance; FTIR, Fourier transform infrared; HOMO, highest occupied molecular orbital; HSA, high-salt medium acetate; hfc, hyperfine coupling constant; MTHF, 2-methyltetrahydrofuran; OD, optical density; PCR, polymerase chain reaction; PMS, phenazine methosulfate; PSI (II), photosystem I (II); SDS, sodium dodecyl sulfate; TAP, Tris-acetate-phosphate; T − S, triplet-minus-singlet; WT, wild type.

10.1021/bi025822i CCC: $22.00
Published on Web 06/14/2002

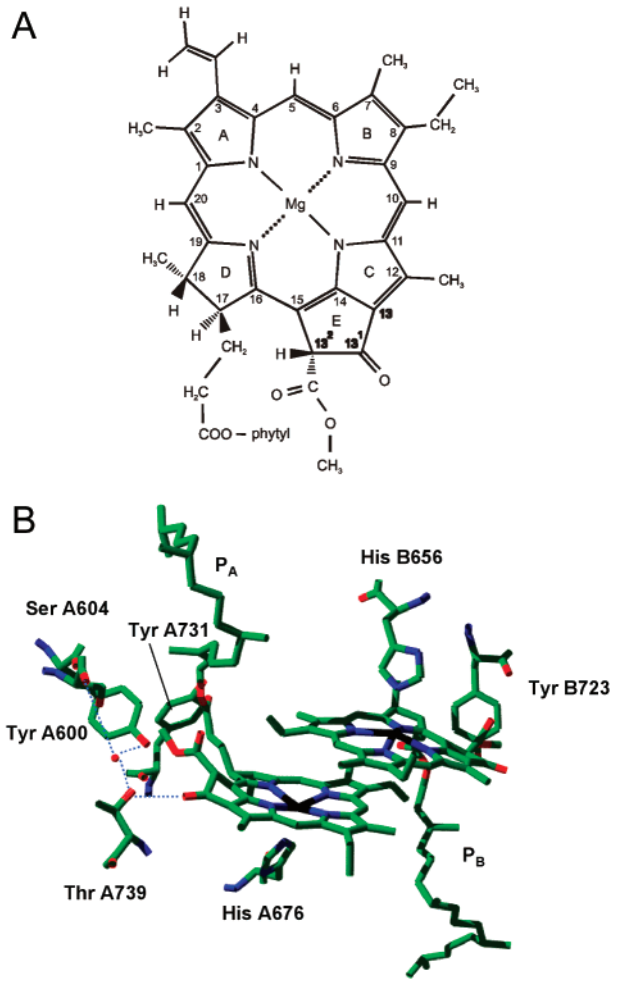

FIGURE 1: (A) Molecular structure and IUPAC numbering scheme for Chl *a*. Chl *a*′ is the C13^2 epimer of Chl *a*. (B) The primary donor P700 with His A676 and His B656 as the coordinating ligands to P700 and Thr A739 as a donor of a putative hydrogen bond to the 13^1-keto group of P_A. Putative hydrogen bonds between P_A, the water molecule, and surrounding amino acid residues are represented with dotted lines. The figure was drawn using the program Swisspdbviewer based on the coordinates of the PSI structure of *S. elongatus* (*3*), with numbering according to *C. reinhardtii*.

(Figure 1A). The coordinating ligand of Chl *a*′ (P_A) is provided by a His from PsaA (His A676) (numbering will be according to *Chlamydomonas* throughout the text), while that of Chl *a* (P_B) is provided by PsaB (His B656). In addition, the interaction of P_A and P_B with the protein environment is different. A hydrogen bond of the 13^1-keto group of P_A to Thr A739 has been proposed (*3*). A water molecule is within hydrogen bonding distance of the hydroxyl group of Thr A739. Ser A604 and Tyr A600 in turn are also within hydrogen bonding distance of the water molecule. It seems as if the water molecule and the surrounding residues are involved in a hydrogen bond network with P_A. In addition, Tyr A731 could form a hydrogen bond with the phytyl ester carbonyl oxygen. These residues are conserved among different species; none of these residues is found on PsaB, and no putative hydrogen bonds to P_B are found (Figure 1B).

The physicochemical properties of the Chls are determined by the electronic structure of their macrocycles and by their substituents. However, evidence that the properties of the cofactors are modified by pigment−pigment and pigment−protein interactions has accumulated. Striking examples are the primary donors of PSI, P700, and PSII, P680. Although both are constituted by Chl *a* molecules, the midpoint potentials differ by ~0.8 V [E_m(P700) = 0.47 V, E_m(P680) = 1.2 V]. Specific interactions with the protein take place via the coordinating ligands and hydrogen bonding with the peripheral substituents of the Chls. The coordinating ligands exert a specific influence on the properties of the redox cofactors, but as they are identical for many cofactors, the wide range of midpoint potentials can hardly be explained by metal coordination. It is very likely that the potentials are modulated by other protein−cofactor interactions, for example, hydrogen bonding. Studies with genetically modified bacterial reaction centers have shown that hydrogen bonding of the protein to the carbonyl group of the 3-acetyl and the 13^1-keto group, which are both part of the conjugated π-system, has a significant influence on the electronic structure and redox potential (*4*−*6*).

In recent years, *Chlamydomonas reinhardtii* has been preferred as a model organism for the analysis of photosynthesis using (site-directed) mutagenesis (for a review, see ref *7*). First, *C. reinhardtii* is able to grow heterotrophically on media with acetate as the carbon source (*8*). Second, with the advent of chloroplast genome transformation and selectable markers, *C. reinhardtii* is easily amenable to genetic manipulation, in particular, to site-directed mutagenesis of chloroplast genome-encoded subunits PsaA, PsaB, and PsaC (*9*−*12*). Site-directed mutagenesis in turn is a powerful tool for identifying the role of individual amino acids and for studying the relationships between the structure and function of photosynthetic reaction centers.

On the basis of the 2.5 Å crystal structure of PSI from *Synechococcus elongatus*, Thr A739 has been suggested to donate a hydrogen bond to the 13^1-keto group of P_A of P700 (*3*) which we assume is also the case for *C. reinhardtii* as this residue is highly conserved among different species. A closer view of the crystal structure reveals that the direction of the side chain of Thr A739 is almost perpendicular to the P_A ring. Due to the size of Thr, the hydrogen bond donating group (OH) seems to be in the correct position for a hydrogen bond to the 13^1-keto group of P_A. At the homologous position in PsaB, Tyr 723 is not capable of a hydrogen bond interaction with P_B as Tyr is larger and its hydrogen bond donating group points in a different direction.

We constructed the mutants TV A739, TH A739, and TY A739 in *C. reinhardtii* and analyzed the effects of the exchange of Thr against Val, His, and Tyr by applying redox titrations and the following spectroscopic techniques: Fourier transform infrared (FTIR), steady state and transient absorption, circular dichroism (CD), electron paramagnetic resonance (EPR), electron nuclear double resonance (ENDOR), and absorption-detected magnetic resonance (ADMR).

MATERIALS AND METHODS

Plasmids and Site-Directed Mutagenesis. Site-directed mutagenesis was performed according to the altered sites mutagenesis procedure (Promega, Heidelberg, Germany) on *psaA*-3. Following mutagenesis and sequencing, a *Cla*I−*Pst*I fragment of *psaA*-3 was subcloned into pKR154 and reintroduced into *C. reinhardtii* CC2696.

Strains, Chloroplast Transformation, and Growth Conditions. As the recipient of the donor plasmids, strain *C.*

reinhardtii CC2696 was used which carries the DS521 cab deficiency mutation and a deletion in *psbA*. PSI complexes isolated from this strain are termed wild type as there are no differences compared to preparations from CC125 (*12*).

Chloroplast transformation was carried out using the biolistics technique essentially as described by Boynton et al. (*13*). Cells were grown in TAP medium (*8*) to a density of approximately 1×10^6 cells/mL and dispersed on TAP plates containing 1.2% agar and 150 μg/mL spectinomycin. Gold particles were coated with 10 μg of donor plasmid DNA and bombarded into the cells using the Biolistics PDS-1000 Particle Delivery System (Bio-Rad). Following bombardment, plates were placed under dim light for 7−10 days until single colonies appeared which were restreaked onto fresh TAP plates supplemented with 150 μg/mL spectinomycin. Total cellular DNA was isolated from the transformed cells. These were scraped up using a toothpick and resuspended in 10 mM Tris-HCl (pH 8), 1 mM EDTA, and 3% SDS and incubated for 15 min. After addition of 500 μL of 10 mM Tris-HCl, 1 mM EDTA, and 70 μL of sodium acetate (3 M), samples were extracted with an equal volume a phenol/chloroform/isoamyl alcohol mixture (25:24:1) and then twice with an equal volume of a chloroform/isoamyl alcohol mixture (24:1). Precipitation of nucleic acids from the aqueous phase was carried out with 1 volume of 2-propanol. DNA was collected by centrifugation and resuspended in an appropriate volume of H_2O, and 1 μL was used as a template for PCR. The amplified DNA was tested by restriction analysis and sequencing. Cells were grown heterotrophically in TAP and HSA medium at 26 °C under low-light conditions.

Preparation of PSI Complexes. As described previously (*12*), cells were harvested and thylakoid preparation was carried out. Isolation of the PSI complex was performed according to the method of Hippler et al. (*14*) with slight modifications. After resuspension of the thylakoid membranes with H_2O at a chlorophyll concentration of 0.2 mg/mL, Pefabloc was added to a final concentration of 1 mM. Membranes were then solubilized only once with 0.9% (w/v) *n*-dodecyl β-maltoside for 20 min at 4 °C while stirring. After addition of NaCl to a final concentration of 50 mM, stirring was continued for an additional 10 min followed by a centrifugation for 30 min at 20000*g*. The supernatant was loaded onto a sucrose density gradient [from 1 to 0.1 M sucrose in 5 mM Tricine-NaOH (pH 7.5) and 0.05% DM] and centrifuged for 16 h at 170000*g*. The lowest band was collected to obtain the PSI particles, diluted with 5 mM Tricine-NaOH (pH 7.5), 0.02% DM, and 100 mM NaCl, and concentrated with an Amicon ultrafiltration cell. Chlorophyll concentrations were determined according to the method of Porra et al. (*15*).

Transient Absorption Spectroscopy. Flash-induced absorbance difference spectra of $P700^{+\bullet}$ and P700 were recorded at room temperature using a laboratory-built flash spectrometer (*16*). PSI complexes were diluted to 10 μM Chl in 20 mM Tricine (pH 7.5), 25 mM $MgCl_2$, 100 mM KCl, 0.02% DM, 5 mM ascorbate, and 10 μM PMS. The samples were then excited with saturating flashes ~15 μs in duration from a Xe flash lamp filtered by colored glass (model CS96-4 from Corning). Measuring light from a 55 W tungsten halogen lamp was passed through a monochromator with a spectral bandwidth of 3 nm, an optical cuvette 1 cm in length, and a combination of interference and edge filters in front of a photomultiplier (EMI 9558BQ) coupled to a transient recorder (Tektronix TDS320). The time course of the absorbance changes was fitted to an exponential decay using an algorithm that minimizes the sum of the unweighted least squares, and difference spectra were constructed from the initial amplitude of the absorbance changes. The difference between the molar extinction coefficients of $P700^+$ and P700 at the peak wavelength was calculated from the flash-induced absorption change of *N*,*N*,*N*,*N*-tetramethyl-*p*-phenylenediamine hydrochloride (TMPD) according to the method of Hiyama and Ke (*17*). TMPD is oxidized by the flash-induced $P700^+$. An extinction coefficient of 12 000 M^{-1} cm^{-1} has been determined for oxidized TMPD at pH 8.0.

For the light-minus-dark absorbance difference spectra at 77 K, PSI complexes were diluted to 10 μM Chl in 20 mM Tricine (pH 7.5), 25 mM $MgCl_2$, 0.02% DM, 5 mM ascorbate, and 60% glycerol; 1.5 mL of the sample was brought into a liquid nitrogen bath cryostat (model DN 1704 from Oxford) under an argon stream at room temperature and dark adapted. The cryostat was then cooled to 77 K with liquid nitrogen and centered in the measuring beam of a Cary 1E UV−vis spectrophotometer (Varian) using a home-built cryostat holder. Spectra were recorded with data intervals of 0.1 nm, a scan speed of 20 nm/min, and a spectral bandwidth of 1 nm. The difference spectra were obtained by subtracting the absorbance spectrum in the dark-adapted state from that after illumination by 20 saturating flashes from a Xe flash lamp. Spectra are normalized to the same bleached area between 600 and 720 nm assuming that the loss of oscillator strength upon photooxidation of P700 is not altered by the mutation.

Circular Dichroism. CD spectra were recorded on a JASCO J-720 spectrometer at room temperature. PSI complexes were diluted to 13 μM Chl in 20 mM Tricine (pH 7.5), 25 mM $MgCl_2$, 100 mM KCl, and 0.02% DM. The solution was divided into two samples. Ferricyanide (1 mM) was added to one sample to oxidize P700, while 5 mM ascorbate and 10 μM PMS was added to the second sample to obtain P700 in the reduced state. Spectra were recorded from 750 to 600 nm at 0.1 nm data intervals with a spectral bandwidth of 2 nm. The spectra of oxidized and reduced samples were measured five times alternating the samples and then averaged. Oxidized-minus-reduced difference spectra were obtained by subtracting the averaged reduced spectrum of the averaged oxidized spectrum.

Redox Titration. To determine the oxidation midpoint potential of P700, the flash-induced absorbance change at 826 nm, associated with oxidation of P700, was measured as a function of the redox potential. Purified PSI complexes were diluted to 20−30 μM Chl in 20 mM Tricine (pH 7.5), 100 mM KCl, 25 mM $MgCl_2$, and 0.02% DM, and the redox potentials were adjusted by adding ferricyanide and ferrocyanide. After each experiment, the potential was measured using a combination Pt/Ag/AgCl electrode (Schott PT5900A) which was calibrated against the redox potential of a saturated solution of quinhydrone as a function of pH. A pH-meter (Knick PHM82) was used to read the redox potential. All redox potentials are given relative to the standard hydrogen electrode (NHE).

ENDOR. ENDOR measurements were performed on a Bruker ESP 300E X-band EPR spectrometer with home-built

ENDOR accessories (*18*). A TM_{110}-type microwave cavity (radio frequency coil arrangement similar to that in ref *19*) was used which provided a good *Q* factor resulting in high ENDOR sensitivity. The sample temperature was controlled using a Bruker ER4111 VT nitrogen flow system. ENDOR experiments were carried out on the cation radical $P700^{+\bullet}$ of PSI complexes in frozen solution at 150 K as described previously (*12*). Samples with PSI complexes from WT and mutants contained between 3 and 5 mM Chl. $P700^{+\bullet}$ was generated by continuous illumination at room temperature with two 150 W halogen lamps equipped with a water filter (2 cm path length) and a 700 nm edge filter for 20 s followed by rapid freezing under illumination.

ADMR Spectroscopy of the P700 Triplet State. Measurements were performed on thylakoid membranes which were diluted to 0.1 mM Chl in 50 mM Tricine (pH 7.5) and 10 mM EDTA. Oxygen was removed using a glucose/glucose oxidase system, and 20 mM dithionite was added under nitrogen. Glycerol was added to a final concentration of 60% (v/v). The samples were then illuminated at room temperature for 5 min with a 1000 W focused tungsten lamp filtered by water and additional heat-absorbing filters. This procedure leads to the reduction of the secondary electron acceptor A_1 and blocking of the electron transfer to A_1. The $P700^{+\bullet}A_0^{-\bullet}$ primary radical pair in turn recombines with a high yield to the triplet state of P700. Illumination continued until 40 K with a 250 W lamp. Measurements were then performed at 1.8 K. The absorption-detected magnetic resonance and the T − S microwave-induced spectra were recorded using the laboratory-built apparatus described in ref *20*.

FTIR. FTIR difference spectroscopy was performed as described by Breton et al. (*21*) with minor modifications. The sample (∼10 μL) containing 3−5 mM PSI was placed onto the depression of a CaF_2 window. After addition of 5 mM sodium ascorbate as a reductant for the primary donor, the droplet was dried under a smooth stream of nitrogen. Before complete dryness, the PSI film was sealed with a second CaF_2 window, yielding a sample with a thickness of 2 μm, minimizing the water absorption. The two windows were fixed with a metal mounting and placed in the sample chamber ($T = 275$ K). The absorbance of the sample in the cell was ∼0.6 at the peak of the amide I absorption band. FTIR spectroscopy was performed with a Bruker IFS 66 V/S FTIR spectrometer. Light-minus-dark FTIR difference spectra were obtained by recording the spectrum of the sample under continuous illumination using a 100 W tungsten halogen lamp with a 590 nm band-pass filter and subtracting the spectrum measured in the dark. To improve the signal-to-noise ratio, ∼10 illumination cycles of the sample each with 256 interferograms were averaged. The FTIR difference spectra were normalized with the vector normalization method based on the spectral regions between 1759 and 1734 cm^{-1}. The spectral resolution was set at 4 cm^{-1}.

RESULTS

Thr A739 donates a putative hydrogen bond to the 13^1-keto group of P_A of the primary electron donor P700 of photosystem I in *C. reinhardtii*. To investigate the influence of this hydrogen bond on the properties of P700, Thr A739 was replaced with Val, His, and Tyr using site-directed mutagenesis. The PSI complexes of the wild type and mutants were isolated and investigated by FTIR, steady state and transient absorption spectroscopy, circular dichroism, EPR/ENDOR, and redox titrations. ADMR measurements were performed on thylakoid membranes.

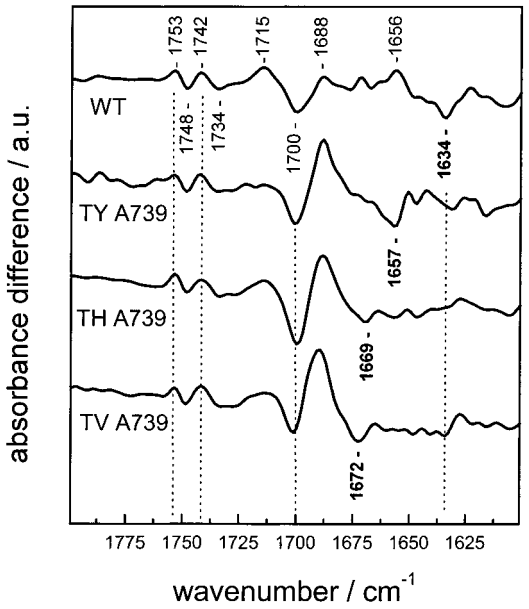

FIGURE 2: Light-induced ($P700^{+\bullet}$ − P700) FTIR difference spectra of PSI complexes from the *C. reinhardtii* wild type and mutants in the 1800−1600 cm^{-1} spectral region. The spectra were normalized with a vector normalization method based on the spectral regions between 1759 and 1734 cm^{-1}.

FTIR Difference Spectroscopy. FTIR is the technique of choice for obtaining direct information about changes in hydrogen bonding to the 13^1-keto group of P_A induced by the replacement of Thr A739 with Val, His, and Tyr. The ($P700^{+\bullet}$ − P700) FTIR difference spectra are shown in Figure 2 for the wild type and mutants. Only vibrational modes affected by the oxidation of P700 contribute to these spectra. Positive amplitudes are due to vibrations associated with the oxidized state, while negative amplitudes are associated with vibrations of the neutral state. The spectral region between 1600 and 1800 cm^{-1} displays bands associated with vibrational modes from the C═O groups of the Chls (*22*−*24*). For the wild type, we observe two large negative bands at 1634 and 1700 cm^{-1} which have been tentatively assigned to Chl *a* 13^1-keto C═O vibrations of P_A and P_B (*22*). Upon formation of $P700^{+\bullet}$, these vibrational modes are upshifted and positive bands appear at 1656 and 1715 cm^{-1}. The two difference signals [positive (+) and negative (−)] detected at 1734 (−)/1742 (+) and 1748 (−)/1753 (+) cm^{-1} have been ascribed to the 13^3-ester C═O vibrations of P_A and P_B (*22*, *25*). For the mutants, the most remarkable results are the upshift of the negative band at 1634 cm^{-1} to 1657 cm^{-1} for TY A739, to 1669 cm^{-1} for TH A739, and to 1672 cm^{-1} for TV A739, and the increase in intensity of a positive band at 1688 cm^{-1}. The upshift of the negative band by 23 cm^{-1} to 38 cm^{-1} is consistent with the expectation that the hydrogen bond to the 13^1-keto group of P_A is broken in the mutants and is the first direct evidence that this band can indeed be ascribed to the 13^1-keto group of P_A. It still remains to be clarified why the position of this band is still downshifted by 20−40 cm^{-1} compared to the 13^1-keto C═O vibration of P_B (1700 cm^{-1}) or Chl *a* in organic solvents (*26*). The positive bands at 1688 cm^{-1} most

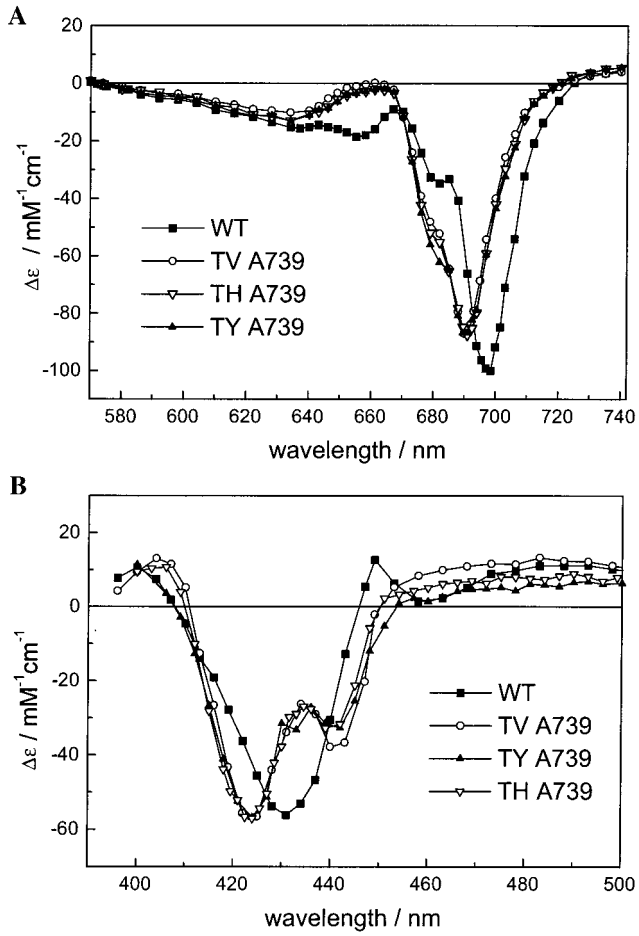

FIGURE 3: Flash-induced ($P700^{+\bullet} - P700$) absorbance difference spectra of PSI complexes from the *C. reinhardtii* wild type and mutants measured at room temperature: (A) the Q_y region and (B) the Soret region. Samples were excited with saturating flashes ~15 μs in duration from a Xe flash lamp (for experimental details, see Materials and Methods).

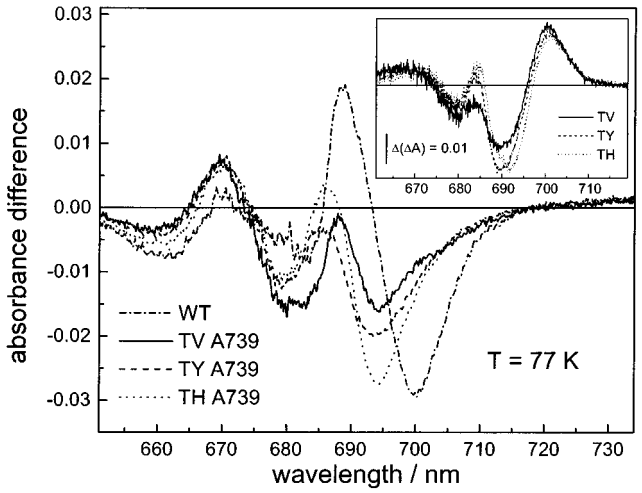

FIGURE 4: Light-minus-dark difference spectra of PSI complexes from *C. reinhardtii* at 77 K. The curves were obtained by subtracting the absorbance spectra in the dark-adapted state from those after illumination with 20 saturating Xe flashes. The spectra are normalized to the same bleached area between 600 and 720 nm (for details, see Materials and Methods). The inset shows double-difference spectra that were generated by subtracting the light-minus-dark absorbance difference spectrum of the wild type from the light-minus-dark absorbance difference spectrum of each mutant for a direct comparison to the wild type.

probably reflect the absorption of the 13^1-keto C═O vibration of P_A in the mutants with P700 in the oxidized state. This would correspond to an upshift of the 13^1-keto C═O vibration of P_A by 30 cm^{-1} upon cation formation which has to be compared to the corresponding upshift by 22 cm^{-1} observed for the wild type.

Absorbance Difference Spectroscopy at Room Temperature and 77 K. Absorbance difference spectra were recorded to investigate the optical features of the primary electron donor. The absorbance changes due to the oxidation of P700 were monitored as a function of wavelength. The molar extinction difference coefficient for the maximum bleaching in the Q_y region ($\Delta\epsilon_{698}$) was determined for WT to be ~100000 M^{-1} cm^{-1}, while for all the mutants, a $\Delta\epsilon_{692}$ value of ~87000 M^{-1} cm^{-1} has been calculated as described by Hiyama and Ke (*17*). The margin of error is estimated to be approximately ±10%. The spectra for the wild type and mutants are shown between 570 and 740 nm in Figure 3A. The main bleaching band of the wild type is located at 698 nm. A blue shift of ~6 nm of the main bleaching band is observed for all the mutants. All spectra exhibit a shoulder on the short wavelength side of the main bleaching band. On the basis of a deconvolution using two Gaussian components, this feature can be attributed to a smaller bleaching band located at 677 ± 1 nm. The ratio between the bleached areas is approximately 5.

In the Soret region, two exponentials are required to fit the time course of the flash-induced absorbance changes. The first phase with a half-life of ~3 ms can be attributed to the reoxidation of F_B^-, while the second phase with a half-life of 60 ms is due to the reduction of $P700^{+\bullet}$. To obtain the ($P700^{+\bullet} - P700$) difference spectrum, the amplitude of the second phase is depicted as a function of wavelength. Compared to the wild type with the main bleaching located at 431 nm, the main bleaching band of the mutants is displaced to 424/425 nm and a second bleaching appears at 440/442 nm (Figure 3B).

At 77 K, absorbance spectra were monitored in the dark-adapted state. After illumination with saturating flashes from a Xe flash lamp, a stable charge separation in $P700^+F_{A/B}^-$ is induced in ~80% of the PSI complexes. The light-minus-dark absorbance difference spectra were obtained by subtracting the absorbance spectra of PSI in the dark-adapted state from those after illumination. They exhibit strong contributions from electrochromic bandshifts induced by the positive charge localized on the oxidized P700. These 77 K ($P700^{+\bullet} - P700$) difference spectra are also strongly affected by the mutations (Figure 4). All spectra have been normalized to the same area between 600 and 720 nm. The spectrum of the wild type is dominated by a strong bleaching at 700 nm and a strong absorbance increase at 689 nm. In addition, some minor absorbance difference bands are observed at 683 (−, very broad), 670 (+), and 660 (−) nm. A plus or minus sign indicates an absorbance increase or decrease induced by the oxidation of P700, respectively. For all mutants, the main bleaching band is displaced 6 nm to the blue. The amplitude decreases strongly in the following order: TH A739 > TY A739 > TV A739. The strong absorbance increase observed in the wild type is also significantly reduced and slightly blue-shifted; for TH A739 and TY

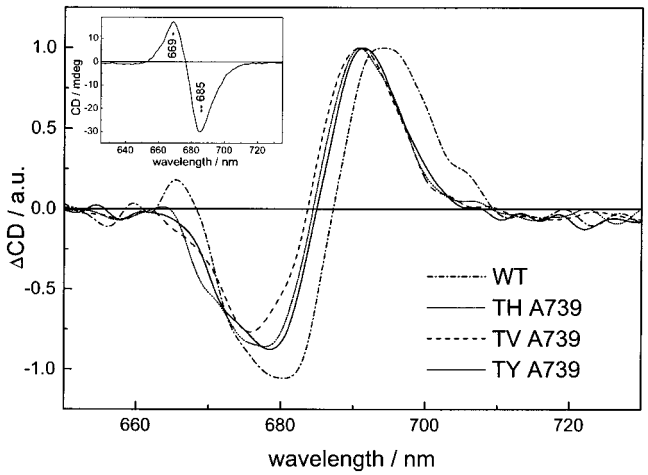

FIGURE 5: Circular dichroism ($P700^{+\bullet} - P700$) difference spectra of PSI complexes from the *C. reinhardtii* wild type and mutants measured at room temperature. The spectra were obtained by subtracting the CD spectra measured with P700 in the reduced state from those measured with P700 in the oxidized state. Oxidation was achieved with ferricyanide. The spectra are normalized to 1 at the positive maximum to allow better comparison. The absolute CD values are 2.1 mdeg for the wild type ($OD_{677} = 1.1$), 3.8 mdeg for TV A739 ($OD_{677} = 1$), 2.2 mdeg for TH A739 ($OD_{677} = 0.8$), and 2.3 mdeg for TY A739 ($OD_{677} = 0.8$). The inset shows the CD spectrum of PSI from the wild type with P700 in the oxidized form.

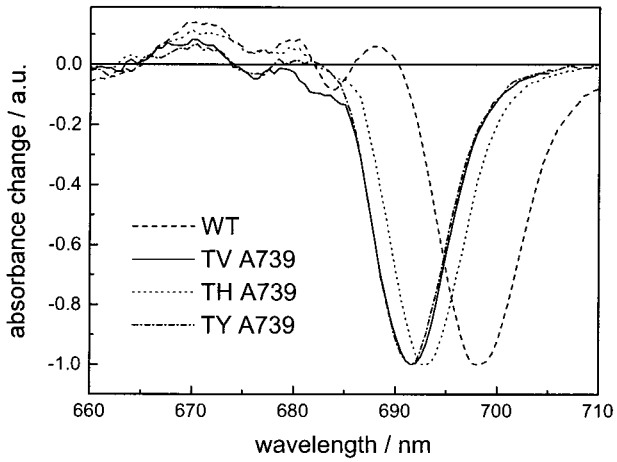

FIGURE 6: Triplet-minus-singlet spectra of P700 from the *C. reinhardtii* wild type and mutants, taken at the maximum of the intensity of the $|D| - |E|$ transitions: 721 (WT), 739 (TV A739), 728 (TH A739), and 737 MHz (TY A739). The modulation frequency was 33 Hz, the microwave power 800 mW, and the optical resolution 1.5 nm, and $T = 1.8$ K (for experimental details, see Materials and Methods).

A739, the blue shift is ~3 nm. For all mutants, an absorbance decrease at 679 nm is observed. Double-difference spectra were generated by subtracting the light-minus-dark absorbance difference spectrum of the wild type from the light-minus-dark absorbance difference spectrum of each mutant for a direct comparison to that of the wild type (Figure 4, inset). The spectral features of the double-difference spectra support the finding that the absorbance band ascribed to the low-energy transition of P700 is shifted. It is clear that the effect is most pronounced for the TV A739 mutant. In addition, a feature at 679 nm is observed for the mutants which is clearly visible in the double-difference spectrum.

Circular Dichroism Difference Spectra. The CD spectrum of PSI from the wild type with P700 in the oxidized form is shown in the inset of Figure 5. The CD spectra obtained with P700 in the oxidized and reduced state are virtually identical (not shown). They display a negative band at 685 nm and a positive band at 669 nm of unequal rotational strength. The excitonic interactions between all chlorophylls of PSI contribute predominantly to the CD intensity since the underlying CD due to the intrinsic chirality of the chlorophylls is usually much weaker. To obtain information about the excitonic coupling between the two chlorophylls constituting P700 and to monitor the changes induced by the mutations, the ($P700^{+\bullet} - P700$) circular dichroism difference spectra were recorded. The CD difference spectrum of the wild type (see the dash−dot line in Figure 5) is dominated by two components located at 694 nm (positive rotational strength) and 680 nm (negative rotational strength). The spectra of the mutants are blue-shifted by ~3−4 nm. Spectra have been normalized to 1 at the positive maximum to allow a better comparison. The spectra are nearly conservative for the wild type and mutants (i.e., each integrated spectrum sums to zero). This suggests that the origin of the prominent CD bands is the excitonic interaction between the reaction center chlorophylls of PSI which is altered upon oxidation of P700. Remarkably, the distance between the positions of the two bands does not change significantly, reflecting the fact that the excitonic coupling is not severely altered in the mutants compared to that in the wild type.

Triplet-Minus-Singlet (T − S) Difference Spectra. The triplet-minus-singlet absorbance difference spectra reflecting the absorbance difference between P700 in its triplet state and its singlet ground state were obtained by ADMR. The minimum of the main bleaching band which has been assigned to the disappearance of the low-energy excitonic band of P700 upon triplet formation is blue-shifted by ~6.5 nm for TV A739 and TY A739 and by ~5 nm for TH A739 in comparison to that of the wild type (Figure 6).

The zero-field-splitting (ZFS) parameters $|D|$ and $|E|$ reflect the energy splittings between the triplet sublevels in a zero magnetic field. The ZFS parameters depend on the spatial distribution of the unpaired electrons in the triplet state over chlorophylls P_A and P_B, and/or the admixture of charge transfer states. At a low temperature (1.8 K), the ZFS parameters of $^3P700$ for the mutants are almost unchanged in comparison to those of the wild type (Table 1). They are virtually identical to those from the monomeric Chl *a* or Chl *a*′ triplet in organic solvents (*27*, *28*; Table 1). This can be taken as evidence that the triplet state of P700 is mainly localized on one of the chlorophylls constituting P700 and that the localization of the triplet state is not significantly altered in the mutants. The slightly larger $|D|$ values of the mutants may be attributed to the removal of the hydrogen bond and/or changes in the polarity of the environment (for discussion of solvent effects, see ref *28*).

Oxidation Midpoint Potential of P700. The midpoint potential (E_m) of P700 is an important property and is assumed to be sensitive to changes in the environment of P700. To determine the oxidation midpoint potential of P700, the flash-induced absorbance change at 826 nm, associated with oxidation of P700, was measured as a function of the potential adjusted by adding varying amounts of ferricyanide and ferrocyanide. The dependence of the amplitude of the

Table 1: ZFS Parameters of the P700 Triplet State from the Wild Type and Mutants from *C. reinhardtii* and the Difference in the Oxidation Midpoint Potential ΔE_m of $P700^{+\bullet}$/P700 between Mutants and the Wild Type

	ZFS parameters[a] [cm^{-1}]		
	$\|D\|$	$\|E\|$	ΔE_m (mV)[b] ($P700^{+\bullet}$/P700)
wild type	0.0280	0.0039	0
TV A739	0.0285	0.0039	-32 ± 4
TH A739	0.0285	0.0041	-9 ± 4
TY A739	0.0286	0.0040	-9 ± 4
^{3}Chl *a*	0.0284	0.0041	−
^{3}Chl *a*′	0.0284	0.0041	−

[a] The error for $|D|$ and $|E|$ is ± 0.0001 cm^{-1}. The $|D|$ and $|E|$ values for ^{3}Chl *a* and ^{3}Chl *a*′ in MTHF have been measured by transient EPR spectroscopy at 10 K. The error for $|D|$ and $|E|$ is ± 0.0002 cm^{-1} (F. Lendzian, L. Fiedor, and W. Lubitz, unpublished results). [b] ΔE_m is the difference $E_{m(mutant)} - E_{m(WT)}$. The absolute value for the oxidation midpoint potential for the wild type in *C. reinhardtii* was determined to 469 ± 6 mV.

absorbance change could be satisfactorily fitted using the one-electron Nernst equation. The midpoint potential of the mutant TV A739 is decreased by 32 ± 4 mV compared to that of the wild type, while for TH A739 and TY A739, it is only lowered by ~9 mV (Table 1). The standard deviation derived from the fits was approximately ±4 mV. The absolute value for the wild type was determined to be 469 ± 6 mV. In this case, the error includes additionally the uncertainty of the calibration of the electrode.

Electron Nuclear Double-Resonance Spectroscopy of P700$^{+\bullet}$. ENDOR spectroscopy was used to characterize the electronic structure of $P700^{+\bullet}$ by resolving the individual proton hyperfine couplings (hfcs) (see ref *29*). The assignment of the obtained hfcs to specific hydrogens of P700 was based on the comparison with ENDOR data reported earlier for Chl $a^{+\bullet}$ in organic solvents and $P700^{+\bullet}$ in PSI single crystals (r*30* and references therein). Käss et al. (*30*) concluded from EPR/ENDOR experiments that the spin density is mainly localized (≥85%) on one of the Chls constituting P700. Later, His 656 in PsaB was identified as the ligand of this spin-carrying Chl of $P700^{+\bullet}$, P_B (*11*, *12*).

Figure 7 compares the ENDOR spectra obtained for $P700^{+\bullet}$ in the wild type and the mutants TV A739, TH A739, and TY A739 in frozen solution. The isotropic hyperfine couplings extracted from the spectra are summarized in Table 2. For comparison, the proton hfcs of Chl *a* measured in organic solvents are given. The largest hfcs in the spectrum [line pairs 17 and 18; numbers refer to the position of the protons according to IUPAC numbering of a Chl *a* molecule (see Figure 1A)] have been assigned previously (*30*) to the β-protons of the spin-carrying Chl *a*. The hfcs of the β-protons at positions 17 and 18 in the mutants are decreased by 0.3−0.5 MHz in comparison to that of the wild type. On the basis of the analysis of ENDOR spectra of $P700^{+\bullet}$ obtained in PSI single crystals, the second largest splittings (line pairs 12) belong to the CH_3 protons at position 12^1 of the chlorin ring (*30*). The ENDOR line pairs at ~3.6 and ~2.9 MHz were assigned to the protons of the two methyl groups at positions 7 and 2, respectively. These resolved hfcs (see Table 2) belong to the spin-carrying Chl, P_B. The remaining small hfcs have not yet been assigned with confidence (*30*).

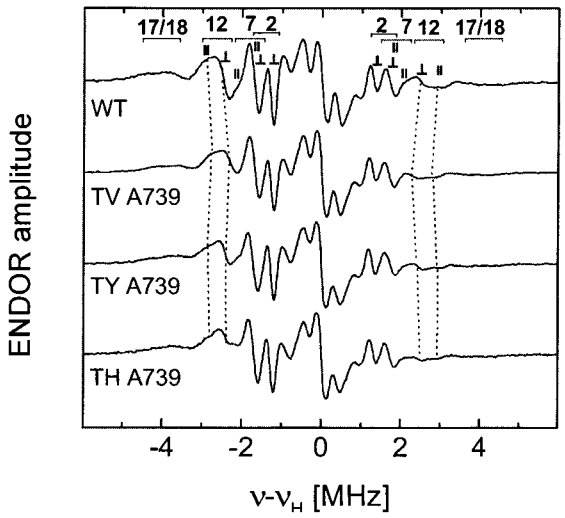

FIGURE 7: ENDOR spectra of $P700^{+\bullet}$ from the *C. reinhardtii* wild type and mutants in frozen solution. The principal components of the hfc tensors for the different protons are indicated for the $A_{||}$ component and the $A_\perp$ component. 12, 12-methyl group; 7, 7-methyl group; 2, 2-methyl group; 17 and 18, β-protons.

Table 2: Hyperfine Couplings of the Methyl Protons (A_{iso}) and of the β-Protons in Megahertz of $P700^{+\bullet}$ from the Wild Type and Mutants of *C. reinhardtii*, in Comparison with Data of Chl $a^{+\bullet}$[a]

	12-methyl group	7-methyl group	2-methyl group	β-protons 17 and 18
wild type	5.32	3.65	2.93	8.7/7.2
TV A739	4.85	3.55	2.83	8.2/6.8
TH A739	5.04	3.7	2.9	8.4/7.0
TY A739	5.04	3.65	2.89	8.4/6.9
Chl $a^{+\bullet}$	7.1	3.0	3.0	10.3/10.1

[a] The values for Chl $a^{+\bullet}$ in CH_2Cl_2 and THF are taken from ref *60*. The error in the hfcs is ±0.1 MHz for the methyl groups and ±0.2 MHz for the β-protons. The A_{iso} values have been calculated from the $A_{||}$ and $A_\perp$ components with the equation $A_{iso} = {}^1/_3(A_{||} + 2A_\perp)$.

In comparison to that of the wild type, the hfc of the methyl protons at position 12 of the spin-carrying Chl P_B (*30*) is decreased for TV A739 by ~0.5 MHz (Table 2 and Figure 7), while for the methyl groups at positions 7 and 2, the changes in the hfcs are close to the error limit. For TH A739 and TY A739, the hfcs of the methyl protons at position 12 are lowered by ~0.3 MHz, while there is again no significant change in the hfcs for the methyl groups at positions 7 and 2. We were not able to resolve any changes in the spectral region that has previously been discussed to contain contributions from the second Chl due to a small fraction of the spin localized on this side (*30*). The decrease of the hfcs of the 12-methyl group and of the β-protons can be taken as an indication for a redistribution of spin density in $P700^{+\bullet}$ compared to that in the wild type.

DISCUSSION

To understand the different biophysical properties of the cofactors in photosynthetic reaction centers, protein−cofactor interaction has been shown to play an essential role, e.g., for the primary donor of bacterial reaction centers (*4*−*6*, *31*). Studies with mutants of the bacterial reaction center demonstrated that hydrogen bonds to the carbonyl groups of the 3-acetyl and the 13^1-keto groups both belonging to the conjugated π-system of the bacteriochlorophylls play an

essential role in modulating the properties of the primary donor. In general, Chls only possess the 13^1-keto group, while the C3 position carries a vinyl group. Thus, a hydrogen bond to the 13^1-keto group would be the most direct way for the protein to interact with a Chl. Inspection of the crystal structure of *S. elongatus* (*3*) reveals threonin at position 739 of the PsaA subunit to be within hydrogen bonding distance of the 13^1-keto group of P_A of P700.

In the study presented here, we exchanged Thr A739, to remove this hydrogen bond, against Val, His, and Tyr for the following reasons. Val is unable to form any hydrogen bond and is nonpolar but should exert only minor steric differences due to the similar side chain volume. His and Tyr are polar amino acids and hydrogen bond donors, but the formation of hydrogen bonds is very unlikely if the steric conditions are taken into account. A Tyr is located at the homologous position in PsaB and forms no hydrogen bond. The effects of the three mutations are indeed similar and can all be explained by the removal of a hydrogen bond (see the discussion below).

Evidence for the Removal of the Hydrogen Bond to the 13^1-Keto Group of P_A of P700. The ($P700^{+\bullet}$ − P700) FTIR difference spectra have been recorded to obtain information about the pigment binding and the pigment−protein interaction of P700. In these spectra, only contributions from vibrational modes affected by the oxidation of P700 are expected; bands associated with P700 appear negative (−), while those associated with $P700^{+\bullet}$ are positive (+). The band pattern of our wild-type spectrum agrees very well with the spectra published previously (*22*, *24*, *32*, *33*), especially the four differential signals detected at 1734 (−)/1742 (+) cm^{-1}, 1748 (−)/1753 (+) cm^{-1}, 1656 (+)/1634 (−) cm^{-1}, and 1715 (+)/1700 (−) cm^{-1} can clearly be resolved. There have been contradictory interpretations concerning the assignment of the 1715 (+)/1700 (−) cm^{-1} differential signal based on investigations of PSI mutants in which the axial ligands of the Mg atoms of P_A or P_B were substituted. Strikingly, mutations of the axial His ligand to P_A led to changes in the 1700 cm^{-1} band (*11*, *24*), while mutations of the central ligand to P_B dramatically disturbed the band at 1634 cm^{-1} which was readily ignored (*11*, *33*) at that time. More recently, the two difference bands at 1656 (+)/1634 (−) cm^{-1} and 1715 (+)/1700 (−) cm^{-1} observed in the wild type (see Figure 2) have been tentatively ascribed to the Chl *a* 13^1-keto C═O vibrations of P_A and P_B, respectively, by Breton and co-workers (*22*). A different assignment has recently been proposed by Hastings et al. (*24*). They conclude that the 13^1-keto C═O vibrations of both Chls of P700 contribute to the strong negative band around 1700 cm^{-1}. However, our results for the mutants offer the possibility of unequivocally deciding between these two different interpretations. The ($P700^{+\bullet}$ − P700) FTIR difference spectra for the mutants TV A739, TH A739, and TY A739 presented in this work lack the negative band at 1634 cm^{-1} and instead exhibit new negative bands at 1657, 1669, and 1672 cm^{-1} (see Figure 2). The band at 1634 cm^{-1} can therefore be assigned with confidence to the 13^1-keto group of P_A which is shifted to higher frequencies by 23 cm^{-1} for TY A739, by 35 cm^{-1} for TH A739, and by 38 cm^{-1} for TV A739 upon removal of the hydrogen bond to the 13^1-keto group of P_A in the mutants. The magnitude of this upshift is consistent with what is expected for the removal of the hydrogen bond (*34*, *35*). The differences between the various mutants can be attributed to the different polarities of the amino acids affecting the 13^1-keto C═O vibration. It should be noted that the wavenumber observed for the 13^1-keto group of P_A after removal of the hydrogen bond is still lower for the mutants [by ∼43 cm^{-1} for TY A739 (1657 cm^{-1}), by ∼31 cm^{-1} for TH A739 (1669 cm^{-1}), and by ∼28 cm^{-1} forTV A739 (1672 cm^{-1})] than the one observed for the non-hydrogen-bonded 13^1-keto group of P_B. These different spectral positions are probably due to the different protein environments. Interestingly, in infrared studies of chlorophyll−water interactions in aliphatic hydrocarbon solvents, Ballschmiter and Katz (*36*) found that the peak at 1700 cm^{-1} attributed to the 13^1-keto group of Chl disappears while an intense peak appears at 1638 cm^{-1}. This band at 1638 cm^{-1} was assigned to a strong keto carbonyl−water interaction whereby the coordination of this water molecule to a Mg atom was thought to be responsible for this unusual strength (*36*). A detailed analysis of the FTIR spectra observed for the wild type and mutants will be presented elsewhere (S. Kohler, H. Witt, O. Hucke, J. Niklas, W. Lubitz, and A. Labahn, manuscript in preparation).

The hydrogen bond network of the binding pocket of P_A has been proposed to be responsible for the selective insertion of chlorophyll *a*′ into the PsaA site of the P700 dimer (*29*). The FTIR results give direct evidence that the hydrogen bond to the 13^1-keto group of P_A is broken in all the mutants. The replacement of Thr with Tyr and His imposes sterical constraints which in turn might lead to the loss of the nearby water molecule. The loss of this water molecule could also be induced by the exchange of Thr against Val due to the hydrophobicity of this amino acid residue. Therefore, we assume that the water molecule is lost in the mutants. This is supported by our data (see the discussion below). It should be noted that the band at 1734 cm^{-1}, which is downshifted in comparison to the free ester carbonyl mode, has been assigned to the 13^3-ester C═O vibration of P_A (*22*, *24*) based on the assumption of hydrogen bonding, probably by the water molecule. However, the crystal structure of cyanobacterial PSI (*3*) reveals a distance between the 13^3-ester C═O vibration of P_A and this water molecule of ∼5 Å which is far too large for a hydrogen bond. As the distance between the water molecule and the bridging oxygen of the carbomethoxy group is only ∼3 Å, a hydrogen bond between this oxygen and the water molecule has been proposed (*3*, *29*). This might be questioned as, if at all, an ether oxygen is thought be a very bad hydrogen bond acceptor.

To determine whether under these conditions chlorophyll *a* has been incorporated into the PsaA site instead of chlorophyll *a*′, an analysis of the pigment composition has been carried out with purified PSI complexes from the wild type and mutants as described previously (*37*). The results revealed about one Chl *a*′ for each PSI for the wild type as well as for the mutants (A. Nakamura and H. Witt, unpublished results). We can therefore exclude the possibility that the altered spectroscopical properties of P700 observed in the mutants are the consequence of a different pigment composition of the dimer in the mutants. The question of why a chlorophyll *a*′ is incorporated into the PsaA site of the P700 dimer still remains to be answered.

Effects of the Mutations on the Spectroscopic Properties of P700. The optical characterization of P700 revealed

significant changes in the spectral features of P700 induced by the mutations. The excitonic interactions between the two Chls constituting P700 (P_A and P_B) and of P700 with other pigments of the reaction center, mainly with the accessory Chls, can be monitored by triplet-minus-singlet absorbance difference spectra (^{3}P700/P700) in a very sensitive way without any contributions due to electrochromic bandshifts. In the low-temperature triplet-minus-singlet spectrum, the main bleaching band has been assigned to the disappearance of the low-energy excitonic band upon triplet formation whereby the excitonic interaction between the Chl carrying the triplet state and its neighboring Chls is lost (*20*, *38*). The features in the region between 660 and 680 nm have been attributed in part to shifts in the absorption of the accessory chlorophylls due to changes in the interaction with P700 upon triplet formation (*20*, *38*). We found that the features are also slightly sensitive to experimental conditions such as redox potential and pH (data not shown). Different suggestions have been made about the assignment for the appearing monomer band of the Chl not carrying the triplet state as well as for the position of the high-energy exciton band (for discussions, see refs *20* and *38*).

In comparison to that of the wild type, the main bleaching band is blue-shifted by ~6.5 nm for TV A739 and TY A739 and by 5 nm for TH A739 (Figure 6). This blue shift could be the consequence of either a blue shift of the Q_y absorption band of P_A due to the removal of the hydrogen bond to the 13^1-keto group or a change in the excitonic coupling between the Chls. As the transition energies of the monomeric pigments constituting the dimer and the excitonic coupling both contribute to the transition energies of the low- and high-energy exciton bands, it is essential to differentiate between these two possibilities. In general, it is a very difficult task to detect exciton splitting using absorption spectroscopy, but this could be accomplished using circular dichroism.

If P700 can be described by an excitonic dimer and the excitonic interactions to the neighboring Chls are only of minor importance, the CD spectrum should exhibit two spectral bands which are of opposite rotational strength. If it is assumed that CD intensity arising from excitonic interactions between the Q_y transition dipoles is much stronger than any other kind of interaction, the CD should be conservative (*39*).

To avoid contributions from the large number of bulk Chls, ($P700^{+\bullet}$ − P700) CD difference spectra have been recorded. Upon oxidation of the dimer, the excitonic interaction and the associated CD vanish. Therefore, the oxidized-minus-reduced CD difference spectrum has been assumed to consist predominantly of the P700 CD, reversed in sign (*40*, *41*). We calculated the CD arising from the excitonic interaction between P_A and P_B (see ref *42* for a brief description of the underlying equations) based on the 2.5 Å structure (*3*). The result is that the low-energy exciton component has positive rotational strength while the high-energy exciton component has negative rotational strength. Note that the ΔCD consists of these components with reversed signs. The measured ($P700^{+\bullet}$ − P700) CD difference spectra for the wild type and mutants (Figure 5), which resemble CD difference spectra obtained with other species (*40*, *41*), exhibit predominantly two components and are nearly conservative. Strikingly, the rotational strengths of the two bands have opposite signs compared to the ΔCD calculated for the P700 dimer. The splitting of the two components is 14 nm in the wild type and mutants. Remarkably, the long wavelength component in the ΔCD is located ~3−4 nm to the blue for the wild type compared to the main bleaching band observed in the T − S spectrum. For these reasons, it is obvious that the spectral features observed in the ΔCD and the absorbance difference spectra cannot be described by a model which takes into account only the excitonically coupled P700 dimer and minor perturbations from the surrounding chlorophylls. Rather, all the exciton interactions between the reaction center Chls, at least those between P_A, P_B, and the accessory chlorophylls, have to be taken into consideration when explaining the ($P700^{+\bullet}$ − P700) difference spectra. This can be rationalized if the coupling strengths between neighboring Chls in the reaction center are comparable in magnitude. That this is the case is supported by calculations of the exciton coupling strengths using the extended dipole approximation. In this approximation, excitonic interaction energies are calculated by summing over the pairwise Coulomb interaction energies of four point monopoles (*42*). Values between 100 and 150 cm^{-1} have been calculated for the interaction energies of neighboring Chls in the reaction center of PSI (*43*). These values correlate well with the 14 nm splitting observed in the ΔCD. It should be noted that for the excitonic interaction energy between P_A and P_B a significantly larger value (≈400 cm^{-1}) is calculated applying the point dipole approximation. For the excitonic couplings between the other pigments, both approximations yield similar values. Due to the short distance between P_A and P_B, it can be expected that in this case the extended dipole approximation is more reliable. Simulations of CD spectra were performed using the extended dipole approximation as described previously (*42*, *43*). To calculate the CD spectrum with P700 in the reduced state, we took into account all the exciton couplings between the six reaction center chlorophylls, each characterized by its individual Q_y transition energy. For the calculation of the CD spectrum with P700 in the oxidized state, P_B has been deleted assuming that the charge is localized on P_B. The calculated oxidized-minus-reduced CD difference spectrum has the qualitative features of the measured one (M. Byrdin and E. Schlodder, unpublished results). The observed blue shift of the ΔCD bands (Figure 5) and of the main bleaching band in the T − S spectra (Figure 6) in the mutants can be explained by a blue shift of the Q_y absorption band of P_A without changing the excitonic coupling between the reaction center chlorophylls. Considering the specific binding pocket of P_A, we suggest that P_A initially has a lower Q_y transition energy than P_B and is blue shifted upon removal of the hydrogen bond to the 13^1-keto group of P_A.

The results derived from the analysis of the ΔCD spectra have consequences for the interpretation of the T − S spectra. The necessity to consider all six reaction center Chls in the analysis of the spectral features might explain the difficulties in assigning an upper exciton band of the P700 dimer and the monomer band arising upon formation of the triplet state. For the analysis of the T − S spectra, additional information about the localization of the triplet state is required. At low temperatures, the $|D|$ and $|E|$ values of ^{3}P700 are very similar to the ones determined for the triplet state of monomeric Chl *a* (*27*, *28*, *44*; Table 1) and Chl *a*′ (Table 1). This can be explained if the triplet state of P700 is localized on one

half of the dimer at low temperatures and does not have charge transfer state admixture. It should be noted that a reduction of the $|E|$ values was observed with increases in temperature, while the $|D|$ value was found to be nearly temperature independent (*44*; J. Niklas and W. Lubitz, unpublished results). The results were explained by a triplet delocalization at higher temperatures over two Chls constituting P700 which have their magnetic *z*-axes parallel and their magnetic *y*- and *x*-axes at an angle of approximately 55°, assuming complete delocalization at room temperature (*44*). In addition, the orientation dependence of the triplet state showed that the plane of the Chl which carries the triplet state is oriented perpendicular to the membrane (*45*); i.e., the triplet state should be localized on P_A or P_B. The possibility that the triplet state is localized on one of the accessory Chls which was shown to be the case in PSII (*46*, *47*) can especially be excluded. The zero-field-splitting parameters $|D|$ and $|E|$ of the PSI mutants studied in this work are almost unchanged, indicating that the spatial distribution of the two unpaired electrons over the chlorophylls P_A and P_B in the mutants is not significantly altered (Table 1).

Information about the localization of the triplet state has been obtained using FTIR experiments with PSI particles from *Synechocystis* sp. PCC 6803 (*22*). The (^{3}P700 − P700) FTIR difference spectrum is dominated by the negative band at 1637 cm^{-1} which was previously attributed to the 13^1-keto C═O vibrations of P_A in the ($P700^{+\bullet}$ − P700) FTIR difference spectrum. The negative band at 1697 cm^{-1} which was ascribed to the 13^1-keto C═O vibrations of P_B in the ($P700^{+\bullet}$ − P700) FTIR difference spectrum is nearly absent in the (^{3}P700 − P700) FTIR difference spectrum. This was taken as evidence that the triplet state is located on P_A (*22*). In contrast, P_B has been proposed to be the Chl carrying the triplet state based on the analysis of the ($P700^{+\bullet}$ − P700) and (^{3}P700 − P700) absorption difference spectra of PSI mutants in which the axial His ligands to P_A and P_B were substituted with several other amino acid residues. Substitution of the central ligands to P_A or P_B led to a blue shift of the main bleaching band in the ($P700^{+\bullet}$ − P700) and (^{3}P700 − P700) spectra. In addition, a positive band located at ∼670 nm in the wild type was shifted upon mutations of PsaB (*12*). On the basis of the assumption that only mutations primarily affecting the Chl which carries the triplet state should become visible in this region of the T − S spectrum, it was concluded that the triplet state is localized on P_B. However, due to the difficulties arising from the necessity to consider all reaction center Chls in the analysis of the absorbance difference spectra, straightforward conclusions cannot be drawn concerning the localization of the triplet state. Nevertheless, the observation that the (^{3}P700 − P700) as well as the ($P700^{+\bullet}$ − P700) spectra are affected in a similar way by each mutation seems to indicate that the triplet state and the positive charge are located on the same Chl. At the moment, it seems difficult to reconcile the different findings with the current state of knowledge.

The ($P700^{+\bullet}$ − P700) absorbance difference spectra recorded at different temperatures confirm that the main bleaching band is blue shifted by ∼6 nm in the mutants TV A739, TH A739, and TY A739 in comparison to that of the wild type. At 77 K, the main bleaching band is not only shifted but also decreased in amplitude to a different extent for the different mutants (see Figure 4). The origin of both effects is the blue shift of the low-energy exciton band. This is obvious from the double-difference spectra (Figure 4, inset) which demonstrate more clearly the spectral differences between the mutants and wild type. They reveal predominantly a similar S-shaped curve for all mutants. As described above, the position of the low-energy exciton band results from the interaction between all the reaction center Chls, and the blue shift in the mutants has been ascribed to an increase in the Q_y transition energy of P_A due to the removal of the hydrogen bond.

The interpretation of the ($P700^{+\bullet}$ − P700) absorbance difference spectra is even more difficult than that of the T − S spectra as the formation of $P700^{+\bullet}$ induces electrochromic shifts of absorbance bands of neighboring Chls. When the temperature is lowered, absorbance changes due to electrochromic bandshifts increase. This might be explained by the narrowing of the absorbance bands and the fact that shielding of the electric field is weakened upon lowering the temperature due to the temperature dependence of the dielectric relaxation (*48*). Therefore, especially at low temperatures, these bandshifts dominate the oxidized-minus-reduced absorbance difference spectra. Two electrochromic band shifts become clearly visible in the ($P700^{+\bullet}$ − P700)-minus-(^{3}P700 − P700) double-difference spectrum of the wild type (not shown): a blue shift with a zero crossing at ∼693 nm and a red shift with a zero crossing at ∼684 nm. The directionality and size of electrochromic band shifts depend on the orientation of the Chls with respect to the position of the charge and distance between them and the dielectric constant of the intervening medium (*49*). On the basis of the predicted directionality of the bandshifts together with the pigment arrangement available from the 2.5 Å structure, the blue shift can be ascribed to the accessory Chls while the red shift can be ascribed to the A_0 Chls. It should be noted that the Q_y absorbance bands of the individual pigments cannot be directly deduced from the observed electrochromic bandshifts which reflect a shift in the resulting exciton bands due to the change of the transition energies of the individual pigments by the electric field.

A comparison with mutant bacterial reaction centers shows that the introduction of a hydrogen bond at the 13^1-keto group (which by analogy is the LH M160 mutant in *Rhodobacter sphaeroides*) leads to a red shift in the Q_y absorption band (*5*, *31*). Also, the bacteriopheophytin on the L side is red-shifted relative to the one on the M side (*50*). The main difference is a hydrogen bond to the 13^1-keto group of BPh_L which is absent for BPh_M. Removal of this hydrogen bond to BPh_L leads to a blue shift of the Q_x band (*51*). So, the blue shift of the main bleaching band is further evidence that the hydrogen bond to the 13^1-keto group of P_A is broken as in the bacterial reaction centers. As explained above, the blue shift of the main bleaching band of P700 itself is a consequence of the blue shift of the Q_y absorption band of P_A. It is very likely that the hydrogen bond is broken in all the different mutants. Nevertheless, the effect of the different mutations on the spectral features is slightly different, so additional effects besides the removal of the hydrogen bond should be taken into account. As mentioned above, the hydroxyl group of Thr A739 is part of a hydrogen bond network (Figure 1). The nearby water molecule involved in the hydrogen bond network together with the residues

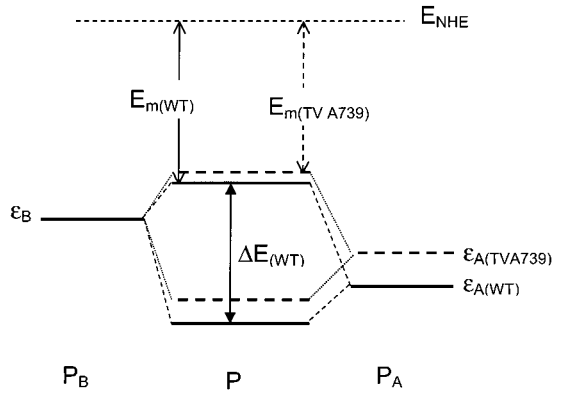

FIGURE 8: Molecular orbital scheme of $P700^{+\bullet}$. E_m denotes the oxidation potential of the dimer, and ϵ_A and ϵ_B are the energies of P_A and P_B, respectively. ΔE is the energetic difference between the resulting super-MOs of *P* and was calculated according to the equation $\Delta E = \sqrt{[(\Delta\alpha)^2 + 4\beta^2]}$, where $\Delta\alpha$ signifies the difference between the HOMO energies of P_A and P_B and β signifies the strength of the electronic coupling. Removal of the hydrogen bond to the 13^1-keto group of P_A leads to an increase in the HOMO energy of P_A to $\epsilon_{A(TV\ A739)}$, resulting in a decrease in the oxidation midpoint potential of P700.

surrounding P_A results in a binding pocket of P_A with polarity that is greater than that of P_B. A consequence of the exchange of Thr against the other residues might be the loss of the hydrogen bond to the water molecule besides the removal of the hydrogen bond to P_A, due to the hydrophobicity of the Val or the size of His or Tyr. Due to this loss of the water molecule, the environment of P_A would become less polar. This effect could also lead to a blue shift, as is observed for the Soret band of porphyrins when they are dissolved in nonpolarizable solvents such as ether in contrast to polarizable solvents such as lutidine (*52*, *53*). The displacement of the main bleaching band to the blue seen in the Soret region confirms this assumption (Figure 3B).

Effects of the Mutations on the Redox Potential and Electronic Structure. The free energy difference between the neutral ground state and the oxidized state of P700 is expressed as the redox potential. The energy of these states can be influenced by the protein environment. The oxidized state is especially affected by electrostatic effects such as charges, permanent dipoles, and the polarizability of surrounding residues. The neutral ground state in turn could be stabilized by hydrogen bonding. The oxidation midpoint potential of $P700^{+\bullet}$/P700 is diminished for all the mutants with TV A739 displaying the largest effect (Table 1). Introduction of a hydrogen bond at the analogous position of Thr A739 in the bacterial reaction center by replacement of Leu M160 with His leads to a redox potential that is more positive than that of the wild type (*6*). Obviously, in bacterial reaction centers as well as in PSI, hydrogen bonding to the 13^1-keto group shifts the redox potential in the same direction.

ENDOR measurements for examining the electronic structure of the oxidized P700 indicate a very asymmetric charge distribution in favor of P_B (*12*, *29*, *30*). The effects of the mutations altering the pattern of hydrogen bonding to P_A can be rationalized within a dimer model (see Figure 8) originally proposed for the primary donor of the bacterial reaction center (*54*−*56*). In the MO scheme (Figure 8), ϵ_A and ϵ_B are the site energies of the isolated monomeric Chls P_A and P_B, respectively, which are assumed to be different ($\epsilon_A - \epsilon_B = \Delta\alpha$). The electronic coupling, β, between the two Chls constituting P700 yields two new super-MOs for the dimer. The energetic difference, ΔE, can be calculated according to the equation $\Delta E = \sqrt{[(\Delta\alpha)^2 + 4\beta^2]}$. The oxidation potential of P700 is related to the HOMO energy level of the dimer and denoted E_m (Figure 8).

Removal of the hydrogen bond between Thr A739 and the 13^1-keto group of P_A is assumed to increase the energy of the HOMO of P_A (ϵ_A), resulting in a destabilization of the dimer HOMO (Figure 8) and a less positive oxidation potential [$E_{m(TV\ A739)} < E_{m(WT)}$]. The differences between the mutants can be rationalized by looking at the different polarizabilities of the residues. If it is assumed that the water molecule has been lost, the polarity of the binding pocket for P_A is decreased but to a lesser extent for the histidine and tyrosine mutants as they are polarizable in contrast to valine.

Another consequence of the increase in the energy of the highest occupied π-orbital (HOMO) of P_A would be a decrease in the site energy difference ($\Delta\alpha$) between P_A and P_B. Therefore, a more symmetric charge distribution and a shift of the spin density toward P_A would be expected.

The spin density distribution can be obtained by measurements of the hfcs and the subsequent assignment to individual molecular positions. To resolve these individual proton hfcs, ENDOR spectroscopy has been applied. A correlation between the degree of localization of the positive charge and the P^+/P redox potential has been demonstrated for mutant bacterial reaction centers (*56*). In the mutant LH M160, ~83% of the spin density is localized on P_L in comparison to the wild type with 68% on P_L (*6*). For bacterial reaction centers, the hfcs of methyl groups 2 and 12 have been assigned for both halves of the dimer (*57*). A spin density shift induced for example by the introduction of a hydrogen bond LH M160 (analogous to Thr A739 in PSI) results in an increase in the hfcs of both methyl groups on one half and concomitantly in a decrease in the hfcs of both methyl groups on the second half (*6*). The hfcs of the methyl protons can be regarded as a measure of the spin density localized on the respective dimer half (*6*, *56*).

ENDOR spectroscopy applied to $P700^{+\bullet}$ leads to the assignment of proton hfcs of the spin-carrying Chl, P_B (*12*, *30*). Unfortunately, an assignment of the hfcs of P_A has not been achieved so far. Compared to that of monomeric Chl $a^{+\bullet}$ in organic solvents, the hfcs of the 12- and 2-methyl groups of $P700^{+\bullet}$ are reduced while the hfc of the 7-methyl group is increased (*30*). Though it is difficult to decide whether these differences between the hfcs of P_B and monomeric Chl $a^{+\bullet}$ in organic solvents reflect a delocalization of spin density between the two halves or a redistribution of spin density within the macrocycle of P_B, it has been argued that at least 85% of the spin density is localized on P_B (*30*). It should be noted that Breton et al. have concluded from FTIR results that the charge in $P700^{+\bullet}$ is essentially equally shared between P_A and P_B (*22*). The peak-to-peak amplitude of the two differential signals attributed to the keto groups of P_A and P_B has been used as an estimate of the charge distribution (*22*). In the model of an electronically coupled dimer, which is supported by the data presented in this work and the mid-IR electronic transition of $P700^+$ (*22*, *24*), it has been argued that the observed upshift in frequency

of the carbonyl stretching frequency is proportional to charge localization (*58*, *59*). However, the relation between charge localization and peak-to-peak amplitude or frequency upshift is not well-established. The possibility that upon cation formation other structural changes affect the carbonyl frequency cannot be excluded, especially if there is a direct interaction between one of the keto groups and its environment via a hydrogen bond. For these reasons, ENDOR spectroscopy has been taken as the method of choice for obtaining information about the localization of the spin and the related positive charge.[2]

ENDOR studies with mutants in which the axial His ligands to P_A and P_B were substituted with several other amino acid residues revealed that only mutations to P_B lead to changes in the spectra whereby only changes of the hfc of the 12-methyl group were resolved. The ENDOR results for the wild type and the mutants TV A739, TH A739, and TY A739 are summarized in Figure 7 and Table 2. Significant decreases in the hfcs of the 12-methyl group and of the β-protons of P_B are observed for the mutants. This is the first time that a mutation affecting P_A leads to changes in the hfcs of the other half of the dimer which may be interpreted as a spin density shift from P_B toward P_A. However, it should be noted that (a) the decrease of the hfcs for the methyl groups at positions 7 and 2 is close to the error limit and (b) any changes in the spectral region that have been argued to contain contributions from P_A are not observed. Since the hfcs of the β-protons are strongly affected by the local geometry (*57*), they cannot be taken as a reliable measure of spin density shifts. However, in all mutants, the decrease in the hfcs of the β-protons correlates with the decrease in the hfcs of the 12-methyl groups. Furthermore, a redistribution of spin density within the macrocycle of P_B due to a local effect at the 12-methyl group of P_B seems unlikely as the 12-methyl group is positioned outside the overlap region and is quite far from the mutated residue. The observed redistribution can therefore be taken as evidence of an electronic coupling between the two halves of the dimer in the wild type as well as in the mutants.

CONCLUSION

Taken together, our data provide evidence that the hydrogen bond to the 13^1-keto group of P_A modulates the properties of P700. The results further imply that the polarity of the binding pocket exerts some influence on P700. (i) The red shift of the Q_y transition energy of P_A caused by the hydrogen bond might be essential for the efficient trapping of the excitation energy. (ii) The oxidation potential of P_A is more positive if the 13^1-keto group of P_A is hydrogen bonded to Thr A739. This is in accordance with observations obtained with the primary donor of bacterial reaction centers (*56* and references therein). The unusually low oxidation midpoint potential of P700 which is ~400 mV more negative than that of Chl *a* in organic solvents can be ascribed in part to the electronic coupling between the two Chls constituting P700 (see Figure 8). (iii) Whereas the cation and at low temperatures also the triplet state of P700 are mainly localized on one of the two Chls constituting P700, evidence is presented that excited singlet states in the reaction center, corresponding to exciton states, are most probably delocalized over the six Chls of the P700 reaction center.

[2] Note that Plato et al. (M. Plato, N. Krauss, P. Fromme, and W. Lubitz, unpublished results) recently showed, on the basis of MO calculations, that the spin density and the charge density distribution in the $P700^{+\bullet}$ dimer are not identical.

ACKNOWLEDGMENT

We are grateful to Marianne Çetin, Heidi Pannier, and Claudia Schulz (Technische Universität Berlin) for excellent technical assistance. The plasmid pKR154 was kindly donated by Dr. Kevin Redding (University of Alabama, Tuscaloosa, AL). We thank Dr. Margitta Dathe (MDC, Buch, Germany) for the opportunity to use the CD spectrometer in her laboratory and for help with the CD measurements. We are particularly indebted to Drs. Friedhelm Lendzian and Martin Byrdin for helpful discussions and Oliver Hucke for providing FTIR data analysis and acquisition software and helpful discussions. We thank Drs. N. Krauss, P. Jordan, W. Saenger, P. Fromme, and H. T. Witt for providing the structural data prior to publication.

REFERENCES

1. Brettel, K. (1997) *Biochim. Biophys. Acta 1318*, 322−373.
2. Golbeck, J. H. (1992) *Annu. Rev. Plant Physiol. Plant Mol. Biol. 43*, 293−324.
3. Jordan, P., Fromme, P., Witt, H. T., Klukas, O., Saenger, W., and Krauss, N. (2001) *Nature 411*, 909−917.
4. Allen, J. P., and Williams, J. C. (1995) *J. Bioenerg. Biomembr. 27*, 275−283.
5. Mattioli, T. A., Lin, X., Allen, J. P., and Williams, J. C. (1995) *Biochemistry 34*, 6142−6152.
6. Rautter, J., Lendzian, F., Schulz, C., Fetsch, A., Kuhn, M., Lin, X., Williams, J. C., Allen, J. P., and Lubitz, W. (1995) *Biochemistry 34*, 8130−8143.
7. Hippler, M., Redding, K., and Rochaix, J.-D. (1998) *Biochim. Biophys. Acta 1367*, 1−62.
8. Harris, E., Ed. (1989) *Chlamydomonas Sourcebook*, Academic Press, San Diego.
9. Webber, A. N., Su, H., Bingham, S. E., Käss, H., Krabben, L., Kuhn, M., Jordan, R., Schlodder, E., and Lubitz, W. (1996) *Biochemistry 35*, 12857−12863.
10. Fischer, N., Setif, P., and Rochaix, J.-D. (1997) *Biochemistry 36*, 93−102.
11. Redding, K., MacMillan, F., Leibl, W., Brettel, K., Hanley, J., Rutherford, A. W., Breton, J., and Rochaix, J.-D. (1998) *EMBO J. 17*, 50−60.
12. Krabben, L., Schlodder, E., Jordan, R., Carbonera, D., Giacometti, G., Lee, L., Webber, A. N., and Lubitz, W. (2000) *Biochemistry 39*, 13012−13025.
13. Boynton, J. E., Gillham, N. W., Harris, E. H., Hosler, J. P., Johnson, A. M., Jones, A. R., Randolph-Anderson, B. L., Robertson, D., Klein, T. M., Shark, K. B., and Sanford, J. C. (1988) *Science 240*, 1534−1538.
14. Hippler, M., Drepper, F., Farah, J., and Rochaix, J.-D. (1997) *Biochemistry 36*, 6343−6349.
15. Porra, R. J., Thompson, W. A., and Kriedemann, P. E. (1989) *Biochim. Biophys. Acta 975*, 384−394.
16. Gerken, S., Dekker, J. P., Schlodder, E., and Witt, H. T. (1989) *Biochim. Biophys. Acta 977*, 52−61.
17. Hiyama, T., and Ke, B. (1972) *Biochim. Biophys. Acta 267*, 160−171.
18. Rautter, J., Lendzian, F., Lubitz, W., Wang, S., and Allen, J. P. (1994) *Biochemistry 33*, 12077−12084.
19. Zweygart, W., Thanner, R., and Lubitz, W. (1994) *J. Magn. Reson. 109*, 172−177.
20. Carbonera, D., Collareta, P., and Giacometti, G. (1997) *Biochim. Biophys. Acta 1322*, 115−128.
21. Breton, J., Thibodeau, D. L., Berthomieu, C., Mäntele, W., Vermeglio, A., and Nabedryk, E. (1991) *FEBS Lett. 278*, 257−260.
22. Breton, J., Nabedryk, E., and Leibl, W. (1999) *Biochemistry 38*, 11585−11592.

23. Hamacher, E., Kruip, J., Rögner, M., and Mäntele, W. (1996) *Spectrochim. Acta, Part A 52*, 107−121.
24. Hastings, G., Ramesh, V. M., Wang, R., Sivakumar, V., and Webber, A. (2001) *Biochemistry 40*, 12943−12949.
25. Kim, S., and Barry, B. A. (2000) *J. Am. Chem. Soc. 122*, 4980−4981.
26. Nabedryk, E., Leonhard, M., Mäntele, W., and Breton, J. (1990) *Biochemistry 29*, 3242−3247.
27. Rutherford, A. W., and Mullet, J. E. (1981) *Biochim. Biophys. Acta 635*, 225−235.
28. Angerhofer, A. (1991) in *Chlorophylls* (Scheer, H., Ed.) pp 945−991, CRC Press, Boca Raton, FL.
29. Webber, A. N., and Lubitz, A. (2001) *Biochim. Biophys. Acta 1507*, 61−79.
30. Käss, H., Fromme, P., Witt, H. T., and Lubitz, W. (2001) *J. Phys. Chem. B 105*, 1225−1239.
31. Williams, J. C., Alden, R. G., Murchison, H. A., Peloquin, J. M., Woodbury, N. W., and Allen, J. P. (1992) *Biochemistry 31*, 11029−11037.
32. Breton, J. (2001) *Biochim. Biophys. Acta 1507*, 180−193.
33. Leibl, W., Brettel, K., Nabedryk, E., Breton, J., Rochaix, J.-D., and Redding, K. (1998) in *Photosynthesis: Mechanisms and Effects* (Garab, G., Ed.) Vol. 1, pp 595−598, Kluwer, Dordrecht, The Netherlands.
34. Lutz, M., and Mäntele, W. (1991) in *Chlorophylls* (Scheer, H., Ed.) pp 855−902, CRC Press, Boca Raton, FL.
35. Mattioli, T. A., Williams, J. A., Allen, J. P., and Robert, B. (1994) *Biochemistry 33*, 1636−1643.
36. Ballschmiter, K., and Katz, J. J. (1969) *J. Am. Chem. Soc. 91*, 2661−2677.
37. Nakamura, A., and Watanabe, T. (2001) *Anal. Sci. 17*, 503−508.
38. Vrieze, J., Gast, P., and Hoff, A. J. (1996) *J. Phys. Chem. 100*, 9960−9967.
39. Tinoco, I., Jr. (1963) *Radiat. Res. 20*, 133.
40. Philipson, K. D., Sato, V. L., and Sauer, K. (1972) *Biochemistry 11*, 4591−4595.
41. Karapetyan, N. V., Shubin, V. V., Rakhimberdieva, M. G., Vashenko, R. G., and Bolychevtseva, Y. V. (1984) *FEBS Lett. 173*, 209−212.
42. Pearlstein, R. M. (1991) in *Chlorophylls* (Scheer, H., Ed.) pp 1047−1078, CRC Press, Boca Raton, FL.
43. Byrdin, M., Jordan, P., Krauss, N., Fromme, P., Stehlik, D., and Schlodder, E. (2001) *Biophys. J.* (in press).
44. Siekmann, I., Brettel, K., Bock, C., Van der Est, A., and Stehlik, D. (1993) *Biochemistry 32*, 4842−4847.
45. Rutherford, A. W., and Setif, P. (1990) *Biochim. Biophys. Acta 1019*, 128−132.
46. van Mieghem, F. J. E., Satoh, K., and Rutherford, A. W. (1990) *Biochim. Biophys. Acta 1020*, 146−152.
47. Diner, B. A., Schlodder, E., Nixon, P. J., Coleman, W. J., Rappaport, F., Lavergne, J., Vermaas, W. F. J., and Chisholm, D. A. (2001) *Biochemistry 40*, 9265−9281.
48. Wong, J., and Angell, C. A. (1976) *Glass structure by spectroscopy*, Dekker, New York.
49. Hanson, L. K., Fajer, J., Thompson, M. A., and Zerner, M. C. (1987) *J. Am. Chem. Soc. 109*, 4728−4730.
50. Zinth, W., Sander, M., Dobler, J., and Kaiser, W. (1985) in *Antennas and reaction centers of photosynthetic bacteria* (Michel-Beyerle, M. E., Ed.) pp 97−102, Springer, Berlin.
51. Bylina, E. J., Kirmaier, C., McDowell, L., Holten, D., and Youvan, D. C. (1988) *Nature 336*, 182−184.
52. Seely, G. R., and Jensen, R. G. (1965) *Spectrochim. Acta 21*, 1835−1845.
53. Belanger, F. C., and Rebeiz, C. A. (1984) *Spectrochim. Acta 40*, 807−827.
54. Plato, M., Lendzian, F., Lubitz, W., and Möbius, K. (1992) in *The photosynthetic bacterial reaction centre II* (Breton, J., and Vermeglio, A., Eds.) pp 109−118, Plenum Press, New York.
55. Parson, W. W., Nabedryk, E., and Breton, J. (1992) in *The photosynthetic bacterial reaction centre II* (Breton, J., and Vermeglio, A., Eds.) pp 79−88, Plenum Press, New York.
56. Müh, F., Lendzian, F., Roy, M., Williams, J. C., Allen, J. P., and Lubitz, W. (2002) *J. Phys. Chem. B 106*, 3226−3236.
57. Lendzian, F., Huber, M., Isaacson, R. A., Endeward, B., Plato, M., Bönigk, B., Möbius, K., Lubitz, W., and Feher, G. (1993) *Biochim. Biophys. Acta 1183*, 139−160.
58. Ivancich, A., Artz, K., Williams, J. C., Allen, J. P., and Mattioli, T. A. (1998) *Biochemistry 37*, 11812−11820.
59. Nabedryk, E., Allen, J. P., Taguchi, A. K. W., Williams, J. C., Woodbury, N. W., and Breton, J. (1993) *Biochemistry 32*, 13879−13885.
60. Huber, M., Lendzian, F., Lubitz, W., Tränkle, E., Möbius, K., and Wasielewski, M. R. (1986) *Chem. Phys. Lett. 132*, 467−473.

BI025822I